Production of positive particles in 8-GeV/c $\pi^- p$ and 18.5-GeV/c $\pi^\pm p$ single-particle inclusive reactions*

P. T. Go, W. D. Shephard, V. P. Kenney, J. M. Bishop, N. N. Biswas, and N. M. Cason
Department of Physics, University of Notre Dame, Notre Dame, Indiana 46556
(Received 19 December 1974)

Inclusive cross sections and invariant single-particle distributions are presented for positive pions and protons produced in 8.05-GeV/c $\pi^- p$ and 18.5-GeV/c $\pi^\pm p$ inclusive reactions. Distributions in p_T^2 and in the longitudinal variables x, y (c.m.) and p_l (lab) are shown. Comparisons are made with inclusive distributions for other particles produced in the same reactions.

We have previously presented data on production of negative pions[1] in 8.05-GeV/c $\pi^- p$ and 18.5-GeV/c $\pi^\pm p$ single-particle inclusive reactions, and of the neutral strange particles[2] K_1^0, Λ^0, and $\bar{\Lambda}^0$, as well as π^0 mesons[3] in the 18.5-GeV/c $\pi^\pm p$ inclusive reactions. We complete our presentation of single-particle inclusive reaction data at these energies with distributions for positive pions and protons produced in the same events.

Exposures at the Brookhaven National Laboratory 80-in. hydrogen bubble chamber yielded 152 000 18.5-GeV/c $\pi^+ p$ pictures, 170 000 18.5-GeV/c $\pi^- p$ pictures, and 50 000 8.05-GeV/c $\pi^- p$ pictures. Subsamples of these pictures were used in the previously published studies of single-particle production.[1-3] All positive tracks in events contained in smaller subsamples of the film were measured and reconstructed in the present study. Results presented here are based on final samples of 19 653 positive tracks (3326 identified protons) in 18.5-GeV/c $\pi^- p$ interactions, 36 159 positive tracks (5894 identified protons) in 18.5-GeV/c $\pi^+ p$ interactions, and 14 546 positive tracks (3700 identified protons) in 8.05-GeV/c $\pi^- p$ interactions. Only events for which all positive tracks were successfully reconstructed are included in the samples. In order to make our results directly comparable with the previously published results we have obtained cross sections and distributions by normalizing our samples for each charge multiplicity to yield the same topological cross sections used in Ref. 1. Corrections have been made for scanning losses of two-prong events with short proton recoils. This normalization procedure corrects final distributions for random track losses in geometrical reconstruction—an effect which becomes more important as the multiplicity increases.

Protons have been distinguished from positive pions on the basis of bubble density. Bubble densities calculated from momenta were printed out for each positive track for which the ratio of p/π^+ bubble densities is expected to be greater than 1.5 (particle momenta < 1.3 GeV/c). The corresponding pictures were examined by physicists, and a choice was made between the p and π^+ possibilities in each case. For positive tracks where the ratio of bubble densities was less than 1.5 no discrimination was attempted. All such tracks have been assumed to be pions. While this will result in the loss of fast protons in the proton sample and consequently in some contamination of the π^+ sample with fast protons, only protons with large four-momentum transfer from the target proton [$|t| \geq 1.25$ (GeV/c)^2] are involved. Only a small fraction of the total number of protons is expected to be involved owing to the known peripherality of high-energy interactions. The ratio of $\pi^+\pi^-$:K^+K^- pair production in the four-body final state at 18.5 GeV/c has been independently determined[4] to be 100:3. We estimate the K^+ contamination in our samples to be at most a few percent. Positive-particle inclusive production cross sections are presented in Table I. In Table II are shown cross sections as a function of charge multiplicity for production of protons with $p_{\rm lab} < 1.3$ GeV/c.

The limitation of our proton sample to protons with $p_{\rm lab} < 1.3$ GeV/c can have important consequences for single-particle distributions. In Fig. 1 are shown, for example, the kinematic regions which may be affected in plots of transverse momentum p_T versus scaling variable x. In the region below the solid (dashed) curves in the backward hemisphere we should have a pure sample of protons (positive pions). To the right of the solid curve nothing about the proton distributions can be determined; to the right of the dashed curve the positive pion sample will include any unidentifiable protons. Since the events included in our samples were not subjected to kinematic fitting, elastic events are included in the single-particle

TABLE I. Inclusive positive-particle production cross sections.

Particle [a]	8.05-GeV/c $\pi^- p$ σ (mb)	18.5-GeV/c $\pi^- p$ σ (mb)	18.5-GeV/c $\pi^+ p$ σ (mb)
all positive [b]	43.39 ± 0.73	50.93 ± 0.82	73.95 ± 1.51
π^+	31.20 ± 0.70	41.12 ± 0.89	61.35 ± 1.46 [c]
p [c]	12.06 ± 0.43	9.59 ± 0.36	12.34 ± 0.48
p (inelastic) [c]	7.01 ± 0.53	5.38 ± 0.40	8.27 ± 0.57

[a] All nondecaying positive tracks with laboratory momenta greater than 1.3 GeV/c are assumed to be pions. Only protons with $p_{\text{lab}} < 1.3$ GeV/c are included in the proton sample.
[b] Includes a contribution from positive strange particles observed to decay in the chamber.
[c] Cross sections are corrected for scanning biases against elastic and two-prong inelastic interactions with very short-range protons.

distributions for protons. No corrections have been made in the following distributions for events with low-momentum protons not found in scanning.

The single-particle inclusive reactions are described in terms of the invariant differential cross section $f(\vec{p}, s) = Ed\sigma/d^3p$, where s is the square of the total c.m. energy and $(\vec{p}, E)$ is the four-momentum of the produced particle. As discussed previously,[1] distributions of $f(\vec{p}, s)$ are most frequently studied in terms of the sets of variables (x, p_T^2), (y, p_T^2), and (p_l, p_T^2), where x is the Feynman longitudinal scaling variable defined[5] as $x = p_L^{\text{c.m.}}/p_{\text{max}}^{\text{c.m.}} \approx 2p_L^{\text{c.m.}}/\sqrt{s}$, where $p_L^{\text{c.m.}}$ is the c.m. longitudinal momentum and $p_{\text{max}}^{\text{c.m.}}$ is the maximum c.m. momentum, y is the c.m. rapidity variable defined as $y = \frac{1}{2}\ln[(E + p_L)/(E - p_L)]$, p_l is the longitudinal momentum in the target rest frame, and p_T^2 is the square of the transverse momentum.

In Figs. 2(a) and 2(b) we present distributions of the structure function

$$F_1(x) = \int_{\text{all } p_T^2} f(x, p_T^2)\, dp_T^2 = \int_{\text{all } p_T^2} \frac{E}{\pi p_{\text{max}}^{\text{c.m.}}} \frac{d\sigma}{dx\, dp_T^2}\, dp_T^2 \approx (2E/\pi\sqrt{s})\, d\sigma/dx$$

as a function of x for π^+ and p, respectively. In Figs. 3(a) and 3(b) are shown distributions of the structure function

$$F_2(p_T^2) = \int_{-1}^{+1} f(x, p_T^2)\, dx$$

as a function of p_T^2 for π^+ and p, respectively. In Figs. 4(a) and 4(b) are shown distributions of

$$G_1(y) = \int_{\text{all } p_T^2} f(y, p_T^2)\, dp_T^2 = \int_{\text{all } p_T^2} \frac{1}{\pi} \frac{d\sigma}{dy\, dp_T^2}\, dp_T^2$$

TABLE II. Cross sections for positive-particle production [a] as a function of charge multiplicity.

Number of charged secondaries	8.05-GeV/c $\pi^- p$ σ (mb) π^+	8.05-GeV/c $\pi^- p$ σ (mb) p	18.5-GeV/c $\pi^- p$ σ (mb) π^+	18.5-GeV/c $\pi^- p$ σ (mb) p	18.5-GeV/c $\pi^- p$ σ (mb) π^+	18.5-GeV/c $\pi^- p$ σ (mb) p
2 [b]	6.49 ± 0.27	7.31 ± 0.40	4.01 ± 0.20	4.90 ± 0.33	9.21 ± 0.68	5.18 ± 0.42
2 (inelastic) [b]	6.49 ± 0.27	2.26 ± 0.50	4.01 ± 0.20	0.69 ± 0.37	5.14 ± 0.74	1.11 ± 0.52
4	16.45 ± 0.41	4.01 ± 0.16	15.08 ± 0.52	3.15 ± 0.13	22.35 ± 0.90	4.69 ± 0.21
6	7.35 ± 0.41	0.72 ± 0.06	14.46 ± 0.57	1.26 ± 0.07	20.07 ± 0.85	2.05 ± 0.10
8	0.89 ± 0.15	0.023 ± 0.009	6.07 ± 0.34	0.25 ± 0.03	7.83 ± 0.43	0.37 ± 0.03
10	0.025 ± 0.020	···	1.31 ± 0.15	0.024 ± 0.008	1.66 ± 0.18	0.042 ± 0.010
12	···	···	0.17 ± 0.07	0.004 ± 0.004	0.21 ± 0.07	0.005 ± 0.004
14	···	···	0.022 ± 0.022	···	0.024 ± 0.019	···

[a] All nondecaying positive tracks with laboratory momenta greater than 1.3 GeV/c are assumed to be pions. Only protons with $p_{\text{lab}} < 1.3$ GeV/c are included in the proton sample.
[b] Cross sections are corrected for scanning biases against elastic and two-prong inelastic interactions with very short-range protons.

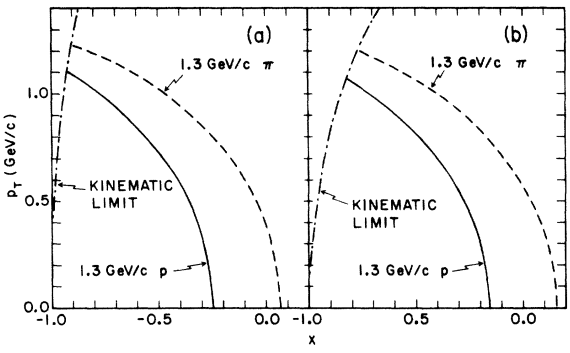

FIG. 1. Plots of p_T versus x are shown for (a) 18.5-GeV/c πp interactions and (b) 8.05-GeV/c πp interactions. The solid curves correspond to protons with laboratory momenta of 1.3 GeV/c; the dashed curves correspond to pions with laboratory momenta of 1.3 GeV/c. The dot-dashed curves indicate the kinematic limits.

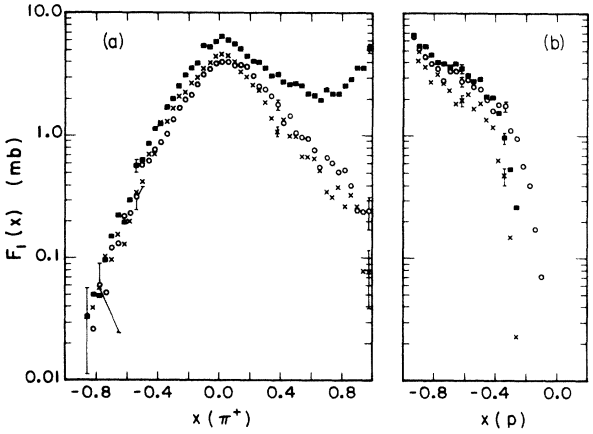

FIG. 2. Distributions of the structure function $F_1(x) = \int f(x, p_T^2)$ as a function of the scaling variable $x = p_L^{c.m.}/p_{max}^{c.m.}$ for (a) π^+ mesons and (b) protons produced in 8.05-GeV/c $\pi^- p$ (○), 18.5-GeV/c (×), and 18.5-GeV/c $\pi^+ p$ (■) inclusive reactions.

for π^+ and p, respectively. In Fig. 5 we present the distribution of

$$H_1(p_l) = \int_{\text{all } p_T^2} f(p_l, p_T^2) dp_T^2$$

$$= \int_{\text{all } p_T^2} \frac{E^{\text{lab}}}{\pi} \frac{d\sigma}{dp_l\, dp_T^2}\, dp_T^2$$

for the π^+. These distributions may be compared to the corresponding distributions for other produced particles in Refs. 1 and 2.

We note that the very rapid falloff of the proton distributions near the upper limits of x and y in Figs. 2(b) and 4(b) must be at least partially due to the method of proton selection. The p_T^2 distributions for protons in Fig. 3(b) must also be affected. If one plots $d\sigma/dp_T^2$ versus p_T^2 for protons in various regions of x, the resulting distributions are qualitatively consistent with an exponential falloff as p_T^2 increases out to the x-dependent kinematic limit shown in Fig. 1. An attempt can be made to correct the proton x distributions with the assumption that the p_T^2 distributions continue to fall off with the same slope as in the observed region, but even this cannot be

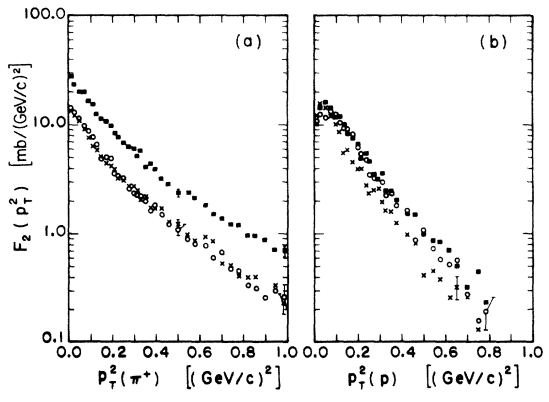

FIG. 3. Distributions of the structure function $F_2(p_T^2) = \int f(x, p_T^2) dx$ as a function of p_T^2 for (a) π^+ mesons and (b) protons produced in 8.05-GeV/c $\pi^- p$ (○), 18.5-GeV/c $\pi^- p$ (×), and 18.5-GeV/c $\pi^+ p$ (■) inclusive reactions.

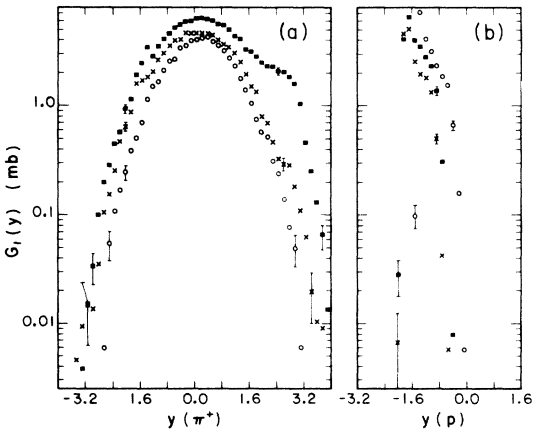

FIG. 4. Distributions of the structure function $G_1(y) = \int f(y, p_T^2) dp_T^2 = (1/\pi)\, d\sigma/dy$ as a function of c.m. rapidity y for (a) π^+ mesons and (b) protons produced in 8.05-GeV/c $\pi^- p$ (○), 18.5-GeV/c $\pi^- p$ (×), and 18.5-GeV/c $\pi^+ p$ (■) inclusive reactions.

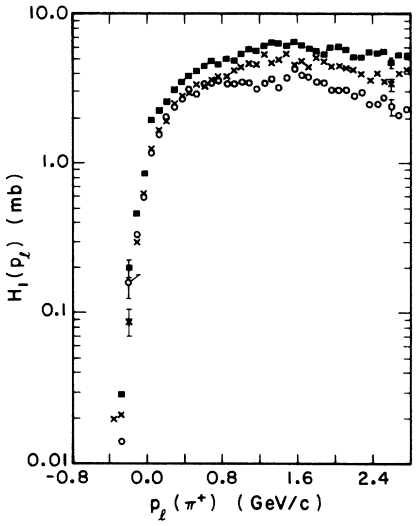

FIG. 5. Distributions of the structure function $H_1(p_l) = \int f(p_l, p_T^2) dp_T^2$ as a function of laboratory-system longitudinal momentum p_l for π^+ mesons produced in 8.05-GeV/c $\pi^- p$ (○), 18.5-GeV/c $\pi^- p$ (×), and 18.5-GeV/c $\pi^+ p$ (■) inclusive reactions.

done in regions of x where the cutoff is varying rapidly.[6]

It is interesting to compare the x distributions for the π^-, π^+, p, K_1^0, Λ^0, and $\bar{\Lambda}^0$ produced in the 18.5-GeV/c $\pi^- p$ and $\pi^+ p$ interactions, as shown in Fig. 6. It is evident that the x distributions are essentially the same for the reactions $\pi^- p \to \pi^-$ and $\pi^+ p \to \pi^+$ over nearly the entire forward hemisphere. For $x<0$, however, they differ significantly, with fewer π^- being produced than π^+. Distributions for the reactions $\pi^- p \to \pi^+$ and $\pi^+ p \to \pi^-$, where the produced pion has a charge different from that of the incident pion, reflect an order-of-magnitude drop in cross sections compared to $\pi^- p \to \pi^-$ and $\pi^+ p \to \pi^+$. The distributions for $\pi^- p \to \pi^+$ and $\pi^+ p \to \pi^-$ are similar in shape, but more π^+ are produced in $\pi^- p$ interactions than π^- in $\pi^+ p$ interactions over the entire range of x, including the forward hemisphere. While some portion of this difference may be due to unidentified protons, it seems improbable that the entire difference could be ascribed to this source. The cross section for $\pi^- p \to p$ is generally lower than

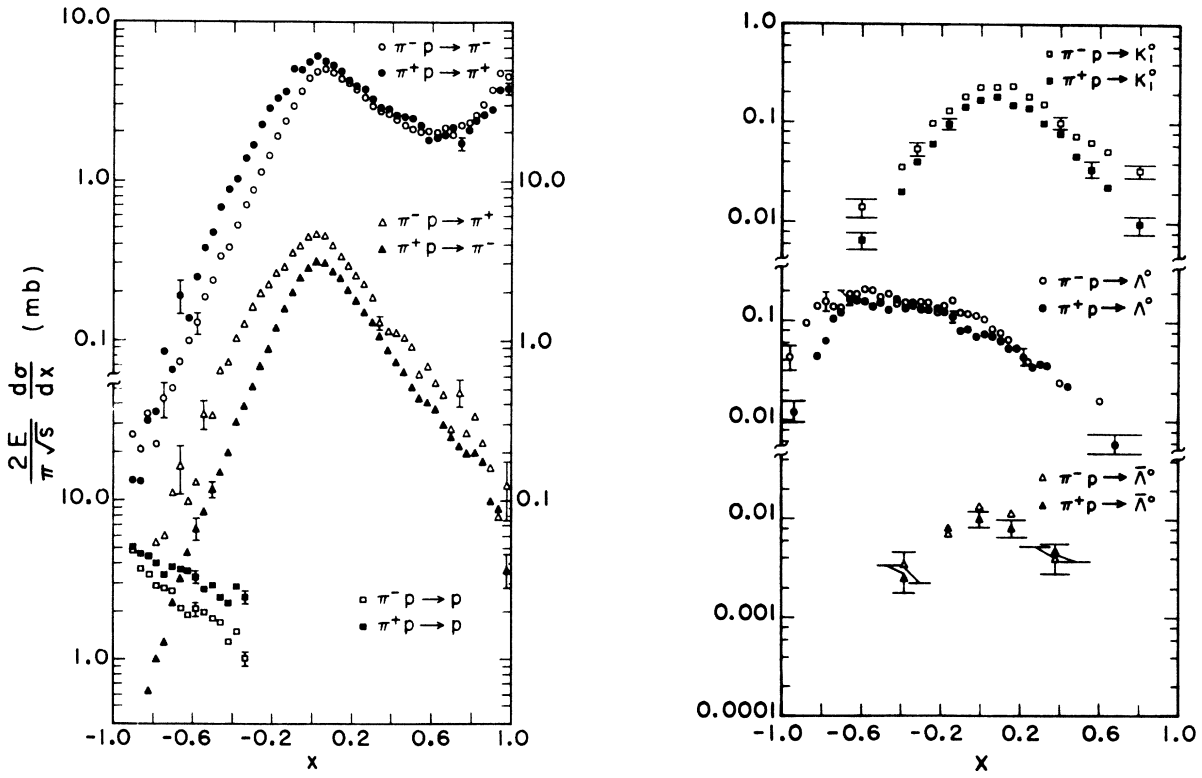

FIG. 6. Distributions of $(2E/\pi\sqrt{s})\, d\sigma/dx$ as a function of $x = 2p_L^{c.m.}/\sqrt{s}$ for π^-, π^+, p, K_1^0, Λ^0, and $\bar{\Lambda}^0$ produced in 18.5-GeV/c $\pi^- p$ and $\pi^+ p$ inclusive reactions. Note that different scales are provided for the different reactions. The proton distributions have been modified, as described in the text.

for $\pi^+ p \to p$. Note that the total cross sections for 18.5-GeV/c $\pi^- p$ and $\pi^+ p$ reactions are 25.38 ± 0.46 and 23.75 ± 0.71 mb, respectively.

Chou and Yang[7] have suggested a language in which the fragmentation reactions

$$\pi^- \xrightarrow[p]{} \pi^- \text{ and } \pi^+ \xrightarrow[p]{} \pi^+,$$

involving no quantum-number exchange, would be equally "favored" fragmentations with large cross sections near $x = 1$. The "disfavored" fragmentation reactions

$$p \xrightarrow[\pi^+]{} \pi^+ \text{ and } p \xrightarrow[\pi^-]{} \pi^-,$$

which involve baryon-number exchange in one case and baryon-number and charge exchange in the other, would be suppressed relative to "favored" fragmentations.[8] It is tempting to ascribe the systematic differences in cross section for extreme forward and backward c.m. directions for the various reactions in Fig. 6 to some such scheme, possibly involving hypercharge or strangeness transfer as well. Alternatively, in a multiperipheral picture the systematics would be associated with the masses of the different particles whose exchange is allowed in these various reactions.[9]

From another point of view, the pions seem to be primarily produced centrally, as are the K_1^0 produced in the $\pi^\pm p \to K_1^0$ reactions. By contrast the proton distribution, and much of the Λ^0 distribution, are consistent with target fragmentation. Interestingly, the $\bar{\Lambda}^0$ appear to be produced centrally, unlike the majority of the Λ^0. Both Λ^0 and $\bar{\Lambda}^0$ distributions are consistent, however, with the hypothesis that the $\bar{\Lambda}^0$'s come from centrally produced hyperon-antihyperon pairs.

The suggested differences in production mechanisms may also be inferred from the representative Biswas plots[10] shown in Fig. 7. In these plots, $p_\parallel(p)$ and $p_\parallel(t)$ are the longitudinal momenta of a secondary particle as observed in the projectile (mass μ) rest frame and in the target (mass M) rest frame, respectively. Particles with small $p_\parallel(p)$ and relatively large $p_\parallel(t)$ correspond to projectile fragmentation. Particles with small $p_\parallel(t)$ and relatively large $p_\parallel(p)$ correspond to target fragmentation. Particles in the central region have approximately equal values for $\mu p_\parallel(p)$ and $M p_\parallel(t)$.

The distributions of $F_2(p_T^2)$ shown in Fig. 3(a) are quite similar to the comparable distributions for π^- mesons published in Ref. 1. The distributions for $\pi^- p \to \pi^+$ show little variation with incident energy for $p_T^2 < 1.0$ GeV/c and exhibit a slope quite similar to the corresponding distributions for $\pi^- p \to \pi^-$ in Ref. 1. The slope of the distributions for $\pi^\pm p \to p$ is influenced by the kinematic cutoffs for our sample of protons. Values of $\langle p_T \rangle$ and $\langle p_T^2 \rangle$ for π^+ mesons[11] are observed to decrease with increasing charged multiplicity, as shown in Table III. A similar decrease was observed previously[1] for π^- mesons.

The variation of inclusive production cross sections with s in the target fragmentation region

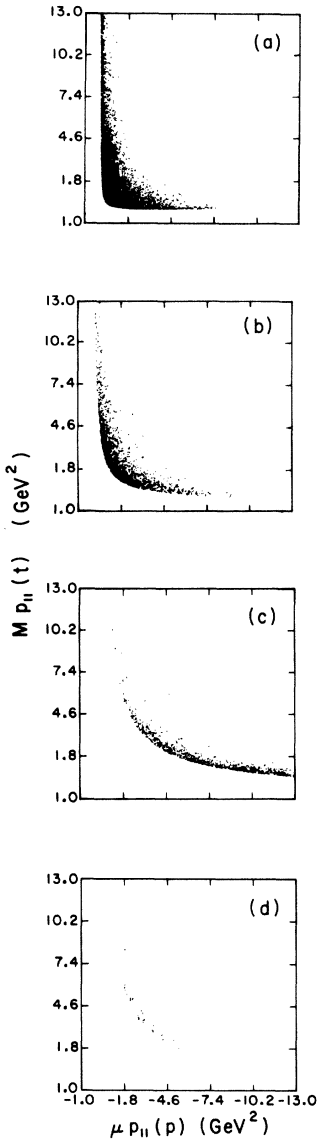

FIG. 7. Representative Biswas plots for the inclusive reactions (a) $\pi^+ p \to \pi^+$, (b) $\pi^- p \to K_1^0$, (c) $\pi^- p \to \Lambda^0$, and (d) $\pi^- p \to \bar{\Lambda}^0$ at 18.5 GeV/c.

TABLE III. Mean transverse momentum [a] and transverse momentum squared for π^+ mesons [b].

Number of charged secondaries	8.05-GeV/c $\pi^- p$	18.5-GeV/c $\pi^- p$	18.5-GeV/c $\pi^+ p$
		$\langle p_T \rangle$ (GeV/c)	
All	0.335 ± 0.002	0.351 ± 0.002	0.365 ± 0.002
2	0.382 ± 0.004	0.406 ± 0.004	0.401 ± 0.004
4	0.338 ± 0.003	0.365 ± 0.003	0.374 ± 0.003
6	0.295 ± 0.004	0.347 ± 0.003	0.360 ± 0.003
8	0.266 ± 0.011	0.310 ± 0.005	0.329 ± 0.004
10	0.297 ± 0.055	0.276 ± 0.009	0.293 ± 0.008
12		0.249 ± 0.024	0.307 ± 0.026
14		0.199 ± 0.042	0.296 ± 0.047
		$\langle p^2 \rangle$ [(GeV/c)^2]	
All	0.180 ± 0.002	0.196 ± 0.003	0.207 ± 0.002
2	0.241 ± 0.004	0.258 ± 0.009	0.237 ± 0.005
4	0.184 ± 0.003	0.213 ± 0.004	0.218 ± 0.004
6	0.127 ± 0.004	0.188 ± 0.003	0.205 ± 0.003
8	0.105 ± 0.010	0.152 ± 0.004	0.167 ± 0.004
10	0.115 ± 0.035	0.119 ± 0.008	0.127 ± 0.007
12		0.088 ± 0.019	0.151 ± 0.026
14		0.050 ± 0.018	0.121 ± 0.033

[a] Quoted errors are statistical errors only.

[b] Protons with $p_{lab} > 1.3$ GeV/c which cannot be identified by bubble density are included in the π^+ sample.

has been the subject of considerable interest.[12] In Fig. 8 we present data on this variation for π^+ production in $\pi^\pm p$ interactions and compare it with data for π^- production presented earlier.

In summary, we have presented single-particle inclusive distributions for positive particles produced in 8-GeV/c $\pi^- p$ and 18.5-GeV/c $\pi^\pm p$ interactions. No extensive analysis of the distributions or of variations over this limited energy range has been included. These data may be compared with similar data at higher energies to study the variation of multiparticle production with incident energy. Effects of the experimental techniques used to separate π^+ and p have been discussed.

We wish to acknowledge the assistance of our colleagues W. L. Rickhoff, R. L. Erichsen, and the Notre Dame scanning and measuring staffs and to thank the staffs of the 80-in. bubble chamber and the AGS at Brookhaven for their help and cooperation. Dr. J. T. Powers and Dr. D. W. Thomas also contributed valuable assistance in the early stages of this study. We also wish to thank the staff of the University of Notre Dame Computing Center for their cooperation.

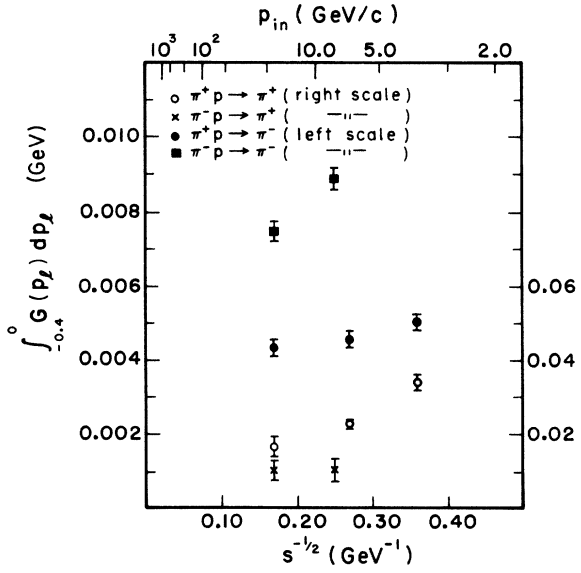

FIG. 8. Plot showing the approach to scaling in the target fragmentation region for π^+ and π^- produced in $\pi^\pm p$ interactions. The ordinate is the integral of the structure function $G(p_l) = \int (E^{lab}/\sigma_T)(d^2\sigma/dp_l\, dp_T{}^2) dp_T{}^2$ over the backward (laboratory) hemisphere.

*Work supported in part by the National Science Foundation.

[1]J. T. Powers *et al.*, Phys. Rev. D 8, 1947 (1973).
[2]P. H. Stuntebeck *et al.*, Phys. Rev. D 9, 608 (1974).
[3]N. N. Biswas *et al.*, Phys. Rev. D 10, 3579 (1974).
[4]E. A. Harrington, Ph. D. thesis, University of Notre Dame, 1970 (unpublished).
[5]At high c.m. energies $p_{\max}^{\text{c.m.}} \to \sqrt{s}/2$. At $s = 16.0$ GeV^2 (8.05-GeV/c πp) $p_{\max}^{\text{c.m.}} = 0.944$ $(\sqrt{s}/2)$; at $s = 35.6$ GeV^2 (18.5-GeV/c πp) $p_L^{\text{c.m.}} = 0.975(\sqrt{s}/2)$. This small difference results in a compression of the data into a narrower x region and a small change in values of $f(x, p_T^2)$ when x is defined as $2p_L^{\text{c.m.}}/\sqrt{s}$ rather than $p_L^{\text{c.m.}}/p_{\max}^{\text{c.m.}}$.
[6]No corrections for cutoffs due to our particle identification procedure have been made in the proton distributions of Figs. 2–4. In Fig. 6 the proton distribution has been corrected in the region $x < -0.36$. No points are shown in Fig. 6 for $x > -0.36$.
[7]T. T. Chou and C. N. Yang, Phys. Rev. Lett. 25, 1072 (1970); T. T. Chou and C. N. Yang, Phys. Rev. D 7, 1425 (1973).
[8]We note that one might also expect the limiting distributions for the "favored" reactions

$$p \xrightarrow[\pi^+]{} p \text{ and } p \xrightarrow[\pi^-]{} p$$

to be the same, as might be the limiting distributions for "unfavored"

$$\pi^+ \xrightarrow[p]{} \pi^- \text{ and } \pi^- \xrightarrow[p]{} \pi^+$$

reactions. The data indicate that these limits have not been reached at the energies considered here.
[9]D. Amati *et al.*, Nuovo Cimento 26, 896 (1962); Chan Hong-Mo *et al.*, Nuovo Cimento 57A, 93 (1968); V. A. Abramovsky *et al.*, in *Proceedings of the XVI International Conference on High Energy Physics, Chicago-Batavia, Ill., 1972*, edited by J. D. Jackson and A. Roberts (NAL, Batavia, Ill., 1973), Vol. 1, p. 389; K. A. Ter-Martirosyan, Phys. Lett. 44B, 377 (1973).
[10]N. N. Biswas, Phys. Rev. D 6, 3127 (1972).
[11]Owing to the limits on p_T imposed by our methods of proton identification values of $\langle p_T \rangle$ have not been calculated for the produced protons. The inclusion of high-momentum protons in the π^+ sample may lead to overestimation of the values of $\langle p_T \rangle$ quoted for π^+ mesons.
[12]M. Alston-Garnjost *et al.*, Phys. Lett. 39B, 402 (1972); M. Jacob, in *Proceedings of the XVI International Conference on High Energy Physics, Chicago-Batavia, Ill., 1972*, edited by J. D. Jackson and A. Roberts (NAL, Batavia. Ill., 1973), Vol. 3, p. 373.

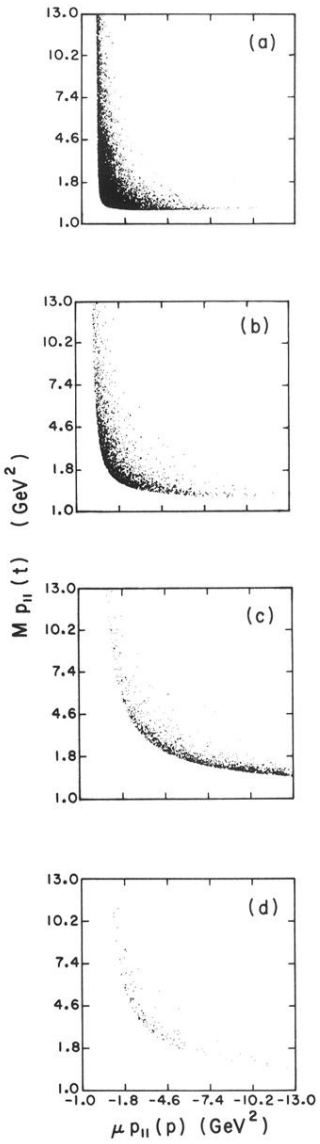

FIG. 7. Representative Biswas plots for the inclusive reactions (a) $\pi^+ p \to \pi^+$, (b) $\pi^- p \to K_1^0$, (c) $\pi^- p \to \Lambda^0$, and (d) $\pi^- p \to \bar{\Lambda}^0$ at 18.5 GeV/c.